



**HAL**  
open science

## Evaluation of Dual Side Cooling System for Prismatic Batteries for Vehicle Applications

Said Madaoui, Bartłomiej Guzowski, Roman Gozdur, Zlatina Dimitrova, Nicolas Audiot, Jocelyn Sabatier, Jean-Michel Vinassa, Franck Guillemard

► **To cite this version:**

Said Madaoui, Bartłomiej Guzowski, Roman Gozdur, Zlatina Dimitrova, Nicolas Audiot, et al.. Evaluation of Dual Side Cooling System for Prismatic Batteries for Vehicle Applications. 36th International Conference on Efficiency, Cost, Optimization, Simulation and Environmental Impact on Energy Systems (ECOS 2023), Jun 2023, Grande Canarie, Spain. pp.2218-2228, 10.52202/069564-0200 . hal-04381384

**HAL Id: hal-04381384**

**<https://hal.science/hal-04381384v1>**

Submitted on 9 Jan 2024

**HAL** is a multi-disciplinary open access archive for the deposit and dissemination of scientific research documents, whether they are published or not. The documents may come from teaching and research institutions in France or abroad, or from public or private research centers.

L'archive ouverte pluridisciplinaire **HAL**, est destinée au dépôt et à la diffusion de documents scientifiques de niveau recherche, publiés ou non, émanant des établissements d'enseignement et de recherche français ou étrangers, des laboratoires publics ou privés.

# Evaluation of dual side cooling system for prismatic batteries for vehicle application

Said Madaoui<sup>a</sup>, Bartłomiej Guzowski<sup>b</sup>, Roman Gozdur<sup>c</sup>, Zlatina Dimitrova<sup>d</sup>, Nicolas Audiot<sup>e</sup>, Jocelyn Sabatier<sup>f</sup>, Jean-Michel VINASSA<sup>g</sup> and Franck Guillemard<sup>h</sup>

<sup>a</sup> Stellantis, Paris, France, [said.madaoui@stellantis.com](mailto:said.madaoui@stellantis.com)

<sup>b</sup> Lodz university of technology, Lodz, Poland, [bartlomiej.guzowski@p.lodz.pl](mailto:bartlomiej.guzowski@p.lodz.pl), <sup>c</sup>

<sup>c</sup> Lodz university of technology, Lodz, Poland, [roman.gozdur@p.lodz.pl](mailto:roman.gozdur@p.lodz.pl)

<sup>d</sup> Stellantis, Paris, France, [zlatina.dimitrova@stellantis.com](mailto:zlatina.dimitrova@stellantis.com)

<sup>e</sup> Stellantis, Paris, France, [nicolas.audiot@stellantis.com](mailto:nicolas.audiot@stellantis.com)

<sup>f</sup> Bordeaux university, Bordeaux, France, [jocelyn.sabatier@u-bordeaux.fr](mailto:jocelyn.sabatier@u-bordeaux.fr)

<sup>g</sup> Bordeaux university, Bordeaux, France, [jean-michel.vinassa@ims-bordeaux.fr](mailto:jean-michel.vinassa@ims-bordeaux.fr)

<sup>h</sup> Stellantis, Paris, France, [franck.guillemard@stellantis.com](mailto:franck.guillemard@stellantis.com)

## Abstract:

Today lithium-ion stands out among the various battery technologies in vehicle applications thanks to their good energy density, low self-discharge and the absence of the memory effect. Nevertheless, lithium-ion batteries pose many challenges such as driving range, lifespan, safety issues and also the charging time which is still significant

In order to reduce the charging time, it is necessary to inject a very high current into the battery which may drastically raise its temperature and thus reduce its lifespan. Today, in most cases, the battery pack of an electric vehicle is cooled through flat cooling plates, mounted either by the lateral or the bottom surfaces. These cooling plates can also be used to warm up the battery in cold weather. But during the fast charge, this configuration poses some problems and can be not efficient enough to cool or heat the batteries.

In this study, a battery module is thermally managed not only by the bottom cooling plate but also by a second cooling plate placed on the busbars. According to simulations and experimental tests regarding one case study, this configuration makes it possible to not only cool the module more quickly by reducing the thermal time constant by 47% but also reduces the battery maximum pick temperature reached with a conventional cooling system by 6°C. It stands out that the top cooling plate acts like a thermal bridge which unifies the temperature inside the battery module and thus support the equal ageing process of the batteries.

## Keywords:

Electric vehicle, batteries, thermal management, cooling plate, thermal gradient, lifespan

## 1. Introduction

The battery pack is the only and main source of energy of an electric car, and to be able to replace an internal combustion engine vehicle, several technical challenges exist that engineers and specialists must face, in order to both increase the autonomy and lifespan while reducing the charging time. Lithium-ion batteries (LIBs) have gradually evolved from a variety of technologies due to their low self-discharge rate, high energy density and lack of memory effect, this type of batteries has revolutionized the energy storage technology and enabled the mobile revolution [1]. Li-ion batteries are available in different shapes and configurations, including cylindrical, prismatic and pouch cells. Temperature is one of the key limiting factors for battery pack performance and lifetime. Temperature heterogeneity inside LIBs causes different electrochemical reaction rates within the cells. This can lead to uneven current density distributions, local State of Charge (SoC) differences and local ageing differences, which may not only accelerate the global ageing, but also reduce the accessible energy of the battery. Temperature rise and spatial temperature gradient minimization inside the cell is among the main thermal challenges during fast charge [2]. Thermal Management Systems (TMS) are employed in majority of vehicles to counter these challenges [3]. A 5°C variation in temperature can reduce the battery pack's capacity by

1.5–2% [4], and its power capabilities by 10% [5]. To improve cooling capability of LIBs, various researchers have incorporated different cooling techniques. Nowadays, liquid cooling, air cooling and phase change material are widely adopted for battery thermal management. Depending on the technical requirements and cost, battery pack manufacturers can use one or several cooling methods. The TMS can be classified into active cooling and passive cooling.

Active cooling consumes extra energy for pumps and fans powering but still more efficient than passive cooling[6]. The active liquid cooling can also be classified into direct-contact and indirect contact. For indirect contact, the liquid is a combination of water and ethylene glycol to avoid liquid freezing at low temperatures inside the cooling plates, while for direct contact, the liquid must be dielectric to avoid any short-circuits. Recently, the direct-contact liquid cooling method has gained increased attention due to its high cooling efficiency [7]. The battery thermal management serves to monitor, control and maintain the optimum operating temperature conditions of a battery. The items that are considered in designing the cooling plate are: (a) the cooling plate should maintain the temperature of batteries at the manufacturer's recommended temperature during normal operation, (b) the cooling plate should dissipate maximum possible heat from the batteries in case of thermal runaway, (c) the coolant pressure drop inside the cooling plate should be minimized, and (d) the size and weight of the TMS should be minimized [8].

Although the above research has achieved remarkable results in battery thermal management, some challenging questions remain: (a) there is little previous literature on battery inner thermal gradient minimization based on both experimental tests and simulations, (b) so far, little work has investigated the benefits of cooling and heating the batteries by putting a cooling plate on top of the battery module, and its role in the battery thermal management.

The aim of this study is to better manage the battery temperature by reducing not only the pick maximum temperature but also the inner thermal gradient, by adding a cooling plate on top of the battery module. The objectives of the present work are as follow:

- perform different experimental tests on a battery module managed thermally in the first case by a bottom cooling plate and then by a top and bottom cooling plates
- compare the results of both technologies in term of thermal management
- build a model and do the calibration using the data acquired during the experimental tests
- use the model to investigate other scenarios in extreme conditions (current and temperature), and of course assess the role of top cooling plate in the battery temperature variation. The last sections conclude and give perspectives on the research topic

## 2. Electrothermal modelling of Li-ion batteries

### 2.1. Battery module model

The battery module consists of 12 prismatic cells connected with busbars to form a 3p4s battery module as represented in the Fig. 1(a). To model the battery module, a fine modeling of its constituents is necessary, by modeling the cells in Fig. 1(b) and also the busbars. Fig.1(c) shows the cover detached from the casing and also the Jelly roll (JR) which represents the heart of the cell and the main part of the battery.

In this section the proposed model is established. With the current, the initial temperature, and the environment temperature as inputs, the model can predict the internal temperature distribution and the state of charge of the battery. The battery module model consists of three sub models, a thermal model, an electrical model based on Electrical Circuit Network ECN and a heat generation model.

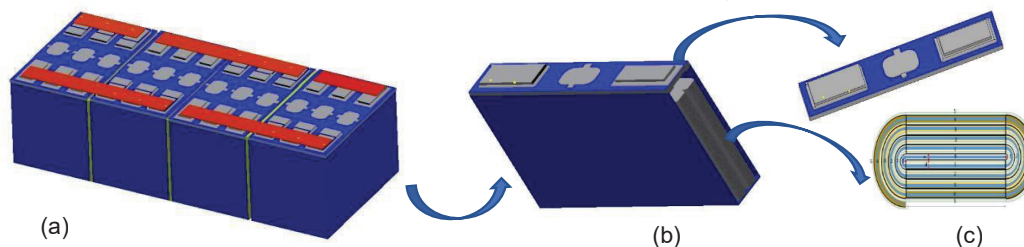


Figure. 1. Structure of the studied system: a) battery module, b) battery cell, c) Cover detached from the casing and JR inside the battery cell

One of the most critical steps for developing battery prognostics solutions is to establish a battery model which enables the auto-maker to simulate battery behavior and interpret battery issues in a form that can be understood by users and designers [9].

Different methods from the electrical, thermal, mechanical and electrochemistry perspectives have been used to establish different battery models, and the dynamic behaviors of the battery regarding different charging/discharging rates and temperatures have been investigated. Among the various battery models, electro-thermal modeling is commonly used to study the relationship between the current and the temperature of battery. The battery electro-thermal model couples the electrical and thermal models closely. The initial inputs of the electrical model are the discharge current, the SOC level and the temperature. The inputs of the electrical model generates heat for the thermal model, this last provides a temperature output signal. Then this temperature signal is fed back to the electrical model, since the new temperature affects the electrical parameters such as the internal resistance.

Generally, the heat generation of the battery  $Q_{gen}$  during charge and discharge contains two parts: reversible and irreversible heats, and it can be expressed by Eq. (1). The entropy change is responsible for the reversible heat  $Q_{rev}$  which can be expressed by Eq. (2), and the irreversible  $Q_{irr}$  heat the heat generated by ohmic resistance is expressed by Eq. (3)

$$Q_{gen} = Q_{irr} + Q_{rev} \quad (1)$$

$$Q_{rev} = I T_b \frac{dOCV}{dT_b} \quad (2)$$

$$Q_{irr} = I^2 R \quad (3)$$

In order to avoid the accumulation of heat at the level of the cell, this heat is often exchanged with the neighboring elements of the cell by conduction  $Q_{cond}$ , or dissipated by different TMS by convection  $Q_{dis}$ . The two modes of heat exchange are detailed in the two equations below Eq. (4) and Eq. (5) respectively

$$Q_{cond} = \frac{(T_{neigh} - T_B)}{R_{th}} \quad (4)$$

$$Q_{dis} = h_{conv}(T_{env} - T_B) \quad (5)$$

The battery temperature is affected by various heat transfer paths. To reduce the battery temperature, part of the heat generated has to be dissipated to the external environment in order to avoid the heat accumulation and thus reduce the temperature raise [10].

### 2.1.1. Battery cell model

The research object is a commercial 67 Ah prismatic battery cell. The battery cell specifications are tabulated in table 1.

Table 1. Specifications of the battery cell

Specification	Value
Cathode material	NMC
Anode material	Graphite
Nominal capacity	67Ah
Cut off voltages	2.8-4.2V
Dimensions	150mm 30mm 100mm
Thermal conductivities	40-2.5-40 W/m.K
Thermal capacity	1200 J/Kg.K

The battery cell is a complex system since it consists of several elements such as JRs, a casing, a cover and electrical insulating films. To finely model the cell, the JRs and the casing are modeled in order to be able to represent the thermal behavior of the battery by having a temperature response at each point of the cell whether at inside or outside. The JR and the casing modeling approaches are now described.

### 2.1.1.1 JR modeling

The challenge is to be able to visualize and quantify the temperature gradients within the cell, while having a model that can be simulated in seconds so that it can be embedded on an electric vehicle. Considering the complex geometry of the JR, it was necessary to design a mesh which makes it possible to represent all the heat exchanges in all directions inside the cell. To successfully reproduce the thermal behaviour of the JR, it is essential to provide a reliable mesh able to represent as good as possible the heat exchanges within the JR, and good assessment of the cell inner thermal gradient. The proposed model consists of meshing the JR in thickness as well as in height. The particularity of this mesh compared to what could be found in literature, is that it takes into account the orthoradial direction which shows that the heat can be exchanged between the meshes by going around the windings. The Fig. 2 shows the proposed mesh by considering the three directions, axial (according to the height of the JR), radial (normal to the winding), orthoradial (parallel to the winding).

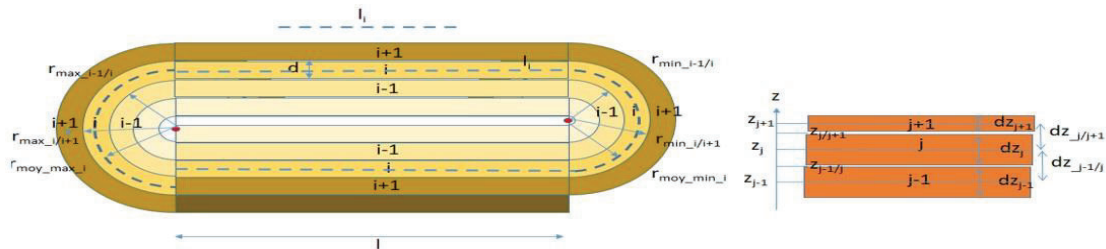


Figure. 2. The proposed mesh of the JR

The JR is obtained by wrapping the electrodes around a hollow space. Each turn is qualified as an elementary layer which is made of different sub layers. Each elementary sub layer has its own thermal conductivity and capacity, its own thickness as well as its own density. All these essential data for the thermal model are taken from literature in absence of having been able to obtain them from the supplier. The JR model is well detailed in [11] with all the equations that represent the physics at the JR level.

To summarize, the heat generated by a mesh  $i,j$  can be calculated according to the following equation:

$$\dot{Q}_{i,j} = R_{30s_{i,j}} I_{i,j}^2 + I_{i,j} T_{i,j} \frac{\partial OC_{V_{i,j}}}{\partial T_{i,j}} \quad (6)$$

### 2.1.1.2 Casing modeling

To get a full model of the cell, the JR have to be linked to the other elements of the cell that surround it, starting with the casing which acts as a thermal bridge between the JR and the external environment. In order to visualize the thermal gradient on the casing, the latter is meshed in height, and each mesh  $j$  of the casing is connected with a mesh  $i_{max,j}$  of the JR. Since the casing is made of aluminium, its specific characteristics are known.

### 2.1.1.3 Busbar modeling

The busbar modeling strategy consists of breaking down the busbar into meshes and assign to each mesh the following Fourier equation:

$$m_{BBi} C_{BB} \frac{dT_{BBi}}{dt} = Q_{generated} + Q_{dissipated} + Q_{exchanged\ by\ conduction} \quad (7)$$

where  $m_{BBi}$  is the mass of a mesh  $i,j$  of a busbar,  $C_{BB}$ , Busbar specific heat capacity, and  $Q_{generated}$  represents the heat generated mostly by Joule effect according to eq. (8),

$$Q_{generated} = \frac{\rho_{BBi}}{S_{BB}} * I^2 \quad (8)$$

$Q_{dissipated}$ , denotes the heat dissipated either by natural or forced convection, and  $Q_{exchanged\ by\ conduction}$  represents the heat that could be exchanged between the busbar and the upper part of the tab and also with the neighbouring meshes of the busbar. The fig. 3 shows the meshed busbar. The heat exchange by radiation was neglected in this paper.



Figure. 3. The meshed busbar connecting six cells

#### 2.1.1.4 Battery module model

Once the battery cell model is well obtained, it is duplicated 12 times to form the 3p4s module model, thus the module is made of 4 blocks of 3 cells each. The cells of the same block are coupled thermally through the busbars as well as through the meshes of their casings. Once the block is built, it is duplicated four times by assuming that the cells are identical, and they have all the same characteristics. Then the four blocks are coupled thermally together through busbars to form what we call a 3p4s battery module.

Figure 4(b) shows the temperature responses of the 12 cells for the current profile represented in the Fig. 4(a). This current profile was chosen to represent both charge and discharge scenarios, and also investigate the electrical resistance variation as function of SoC.

The hypothesis are not detailed for this part, because the goal is to show that the model allows to have the temperature responses of the twelve cells for a given current profile, the assumptions will be detailed in the part dedicated to (results and comparison).

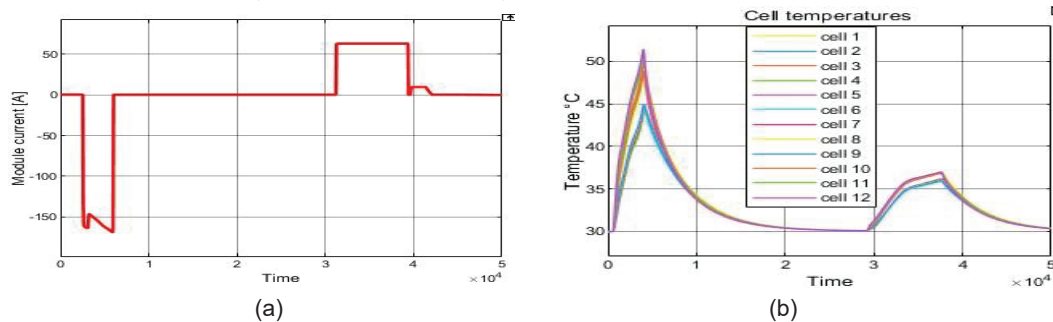


Figure. 4. Simulation results after building the model: a) Input current, b) cells temperatures

## 2.2. Model calibration

Before starting the calibration of the module model, some assumptions have been considered.

### 2.2.1. Assumptions

The following assumptions have been made for model calibration

- the cells inside a module are all identical
- the presence of thermal spacers between the blocks means that the only thermal path between the block of cells becomes the busbars
- the electrical resistances between the busbars and the tabs are considered null.
- the temperatures of the air in the climatic chamber and of the liquid circulating inside the plates are constant throughout the test.
- the initial and boundary conditions of the model are supposed to be suitable to the experiment conditions

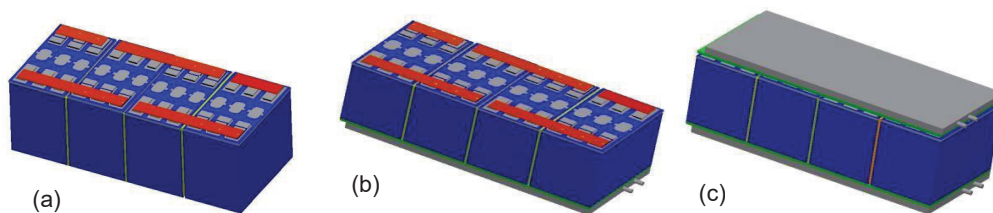


Figure.5. Battery module thermal management: a) module without any cooling plate, b) module with bottom cooling plate, c) module with top and bottom cooling plates

### 2.2.2. Battery module without any cooling plate

In order to calibrate the model detailed above, some electrothermal tests have been carried out on the 3p4s module. The first tests have been carried out on the module without any cooling plate as shown in the Fig. 5(a), and the goal is to reproduce correctly the thermal and electrical responses of the twelve cells. At first the battery module has been put in a climate chamber. So, the first parameter to be determined was the heat exchange coefficient  $h_{conv}$ . The second parameter was the contact electrical resistances between the electrical load and the battery module terminals. These contact electrical resistances can play a very important role in the thermal behavior of the batteries, especially when the contact is bad.

### 2.2.3. Battery module with a top and bottom cooling plate

The same electrothermal tests have been carried out, first on the battery module coupled to a bottom cooling plate (first case see the Fig. 5(b)) and then on the battery module coupled to the top and bottom cooling plates (second case as shown by the Fig. 5(c)).

Once the data acquisition is done through thermocouples, the goal was to assess the benefits of adding the cooling plates and then compare the technologies in term of efficiency in thermal management of the batteries. At the model level the only parameters that had to be determined in order to reproduce the thermal responses of the cells were: (a) the thermal resistances between the bottom cooling plate and the bottom surfaces of the cells for the first case and (b) the thermal resistance between the top cooling plate and the busbars for the second case.

## 3. Measurement setup and test procedures

A dedicated test stand has been developed to assess the efficiency of the cooling system extended with a cooling plate through the upper surface on which the connection electrodes are installed. All experimental tests were performed for the same battery module at the same, strictly controlled conditions. Each time, preconditioning procedure was preceded to reach the same initial state of charge and state of health of the tested battery module before tests. The test stand consists of the Li-Ion battery module, the thermal management system, charging/discharging system and a control and acquisition system.

### 3.1. Tested battery module

For the evaluation of the cooling improvements, the high-power battery module has been selected. The battery module was made of 12 Li-Ion prismatic cells connected in the 3s4p setup. Technical parameters of the cells were listed in subsection 2.1.

### 3.2. Thermal Management system and thermal test procedure

The thermal management system consists of two water cooling plates, water chiller and thermal chamber. As shown in Fig. 6, the battery module was placed in the thermal chamber. The bottom dedicated cooling plate was connected in parallel with top cooling plate and supplied from the chiller CW-6100AN. The inlet temperature of purified water was control by the chiller. Cooling plates were integrated with battery module through 3 mm thick thermal pad.

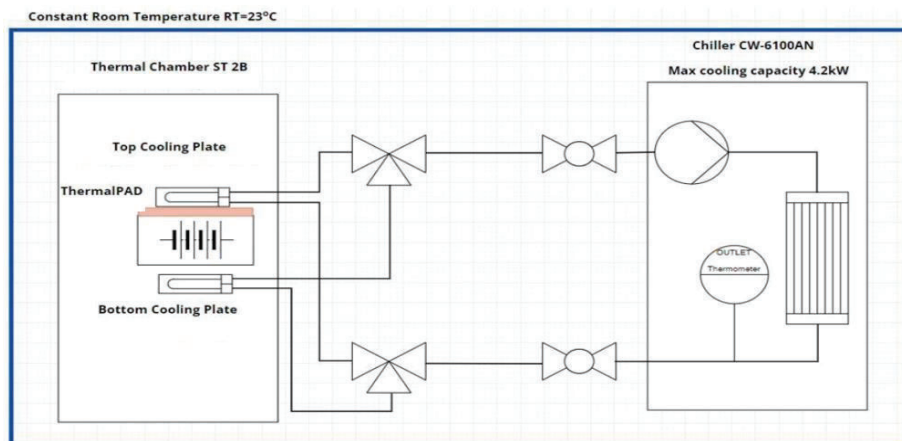


Figure 6. The diagram of the thermal management system

## 4. Experimental results

### 4.1. Charging battery module

The thermal response of the battery module was measured during charge test, where coolant temperature was set at  $T_C = 20\text{ }^\circ\text{C}$  and ambient temperature was  $T_A = 25\text{ }^\circ\text{C}$ . The thermal response of battery module with only bottom cooling plate during the charge test is shown in Fig. 7. The temperature of a bottom cooling plate was measured by sensor labeled as  $T_{cp}$  which was placed between battery module and cooling plate. Temperature inside climate chamber was recorded by two sensors TA and TA1. Time constant for this process equals to  $\tau = 5700\text{ s}$ . Maximum temperatures were recorded on terminals of tested module. The temperature  $49.6\text{ }^\circ\text{C}$  was recorded by sensor 37. The highest temperature recorded inside battery module exceeded  $43\text{ }^\circ\text{C}$  (sensor 19, sensor 20, sensor 21) and it was recorded during highest charge current  $I_{CHA} = 190\text{ A}$ . On the other hand, the lowest temperature was recorded on side walls of battery module, and it did not exceed  $37\text{ }^\circ\text{C}$  (sensor 43, sensor 45, sensor 41 and sensor 40).

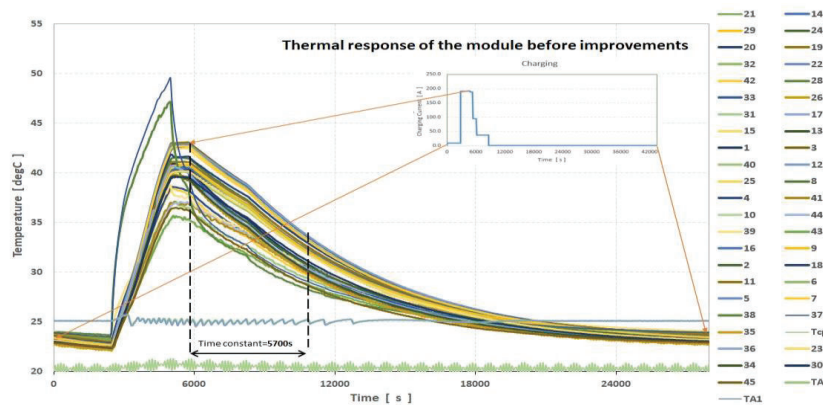


Figure 7. Thermal response of battery module with bottom cooling plate during charge process, where  $T_A = 25\text{ }^\circ\text{C}$ ,  $T_C = 20\text{ }^\circ\text{C}$

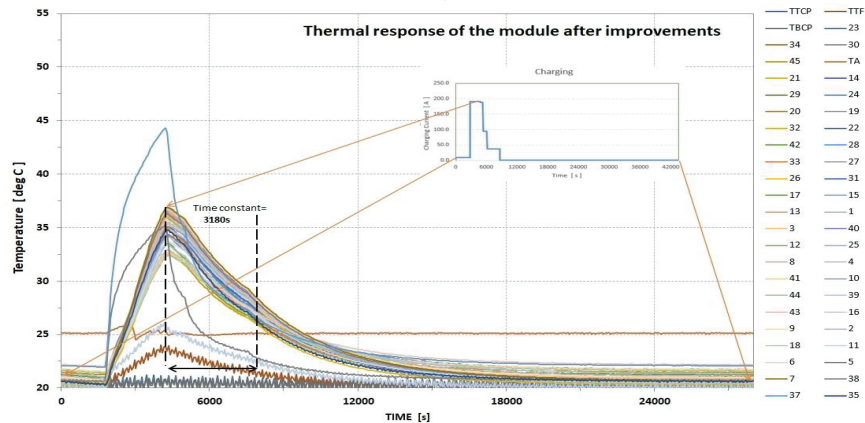


Figure 8. Thermal response of battery module with top and bottom cooling plate during charge process, where  $T_A = 25\text{ }^\circ\text{C}$ ,  $T_C = 20\text{ }^\circ\text{C}$

Additional top cooling plate caused drop of maximum temperature measured on terminals to  $44\text{ }^\circ\text{C}$  (sensor 37) and  $35\text{ }^\circ\text{C}$  (sensor 38) as shown in Fig. 8, and also the drop in the average temperature of battery module. Highest temperature recorded by sensors placed inside the battery module (e.g. sensor 19, sensor 20, sensor 21) was  $37\text{ }^\circ\text{C}$  and it was lower by  $6\text{ }^\circ\text{C}$  in comparison to the test with only one cooling plate. Temperature on the side walls of battery module did not exceed  $33\text{ }^\circ\text{C}$ . Cooling time constant was decreased by 44% from  $\tau = 5700\text{ s}$  to  $\tau = 3180\text{ s}$ . Another advantage of adding the top cooling plate is clearly visible with a smaller temperature discrepancy inside the battery module from

7°C to 3.5°C. Therefore, the aging process of batteries inside the battery module can be easily controlled. Average relative improvement rate equals to 21%. The highest improvement (37%) was recorded for sensor 38 placed on one of terminals. Average relative improvement inside the battery module was around 19%.

The thermocouples described above are shown in the figure below.

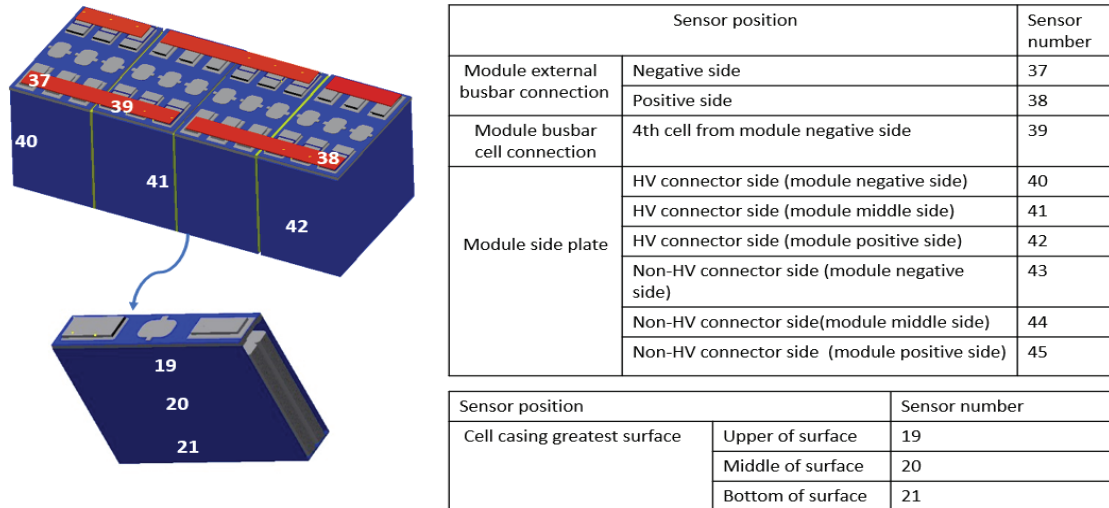


Figure 9. Layout of the temperature sensors

#### 4.2. Discharging battery module

After charging tests, the discharge test was conducted with  $T_A = 25^\circ\text{C}$  and  $T_C = 30^\circ\text{C}$ . In Fig. 10, thermal response of battery module with only bottom cooling plate during the investigation is given. The same test was conducted once again for battery module equipped with bottom and top cooling plates. Thermal behavior of the module is shown in Fig. 11. Differences in C-rate profile caused longer time constant for cooling process which was equaled to  $\tau = 7260\text{s}$ . For this case study, the time constant was decreased by 55% in the tests with two cooling plates. Maximum temperatures before and after adding the top cooling plate ( $45^\circ\text{C}$  and  $43^\circ\text{C}$ ) were recorded on terminals of battery module. Maximum recorded temperature after improvement inside the battery module dropped by  $2^\circ\text{C}$ , but on the other hand the temperature inside the module was more uniform in a test with top and bottom cooling plates. At  $t = 6000\text{s}$ , the temperature difference measured inside the battery module and on external walls dropped by half from  $5^\circ\text{C}$  to  $2.5^\circ\text{C}$ . It stands out that the average relative improvement rate was 31%.

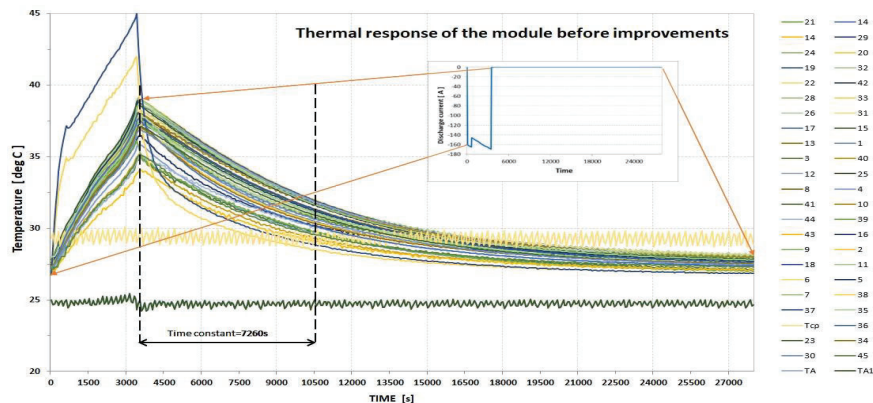


Figure. 10. Thermal response of battery module with bottom cooling plate during discharge process, where  $T_A = 25^\circ\text{C}$ ,  $T_C = 30^\circ\text{C}$

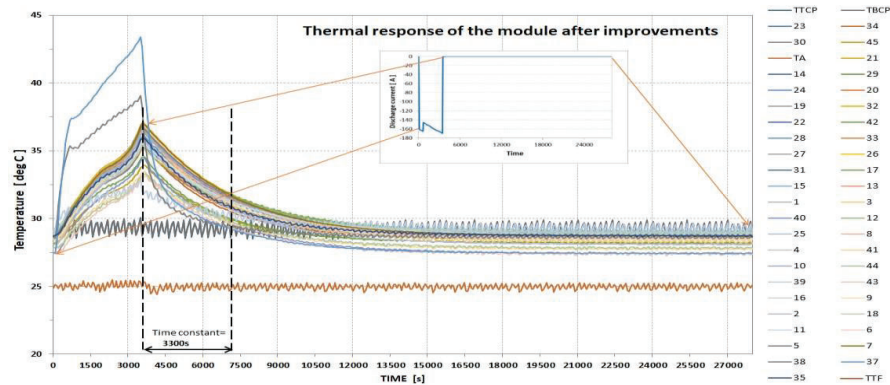


Figure. 11. Thermal response of battery module with top and bottom cooling plate during discharge process, where  $T_A = 25\text{ }^{\circ}\text{C}$ ,  $T_C = 30\text{ }^{\circ}\text{C}$

## 5.Results comparison

Different electrothermal tests have been carried out to validate the battery module model. In this paper for the sake of brevity, only one test will be discussed.

In this test, the current profile used to validate the model is shown in Fig. 12(a). The advantage of this current profile is that it allows to scan the entire SoC range in order to check the lookup-tables of the electrical resistances of the batteries during charge and discharge as well as that of the OCV, this current profile also permits to assess the effect of the current amplitude on the thermal and electrical responses of the batteries.

The experimental test conditions have been taken into consideration and some simplifying assumptions and boundary conditions have been set in order to simulate the model and compare the obtained signals with those of the experiment:

- the module is cooled with the top and bottom cooling plates
- the air temperature is set at  $25\text{ }^{\circ}\text{C}$  and coolant temperature at  $20\text{ }^{\circ}\text{C}$
- the initial temperature is set at  $20.7\text{ }^{\circ}\text{C}$
- one cell of the module is targeted to do the comparison between the model and the experiment, and the considered thermocouple is fixed at the center of the great surface of this battery

The Fig. 12(b) shows the temperature response of the model in red compared to the temperature given by the thermocouple in black.

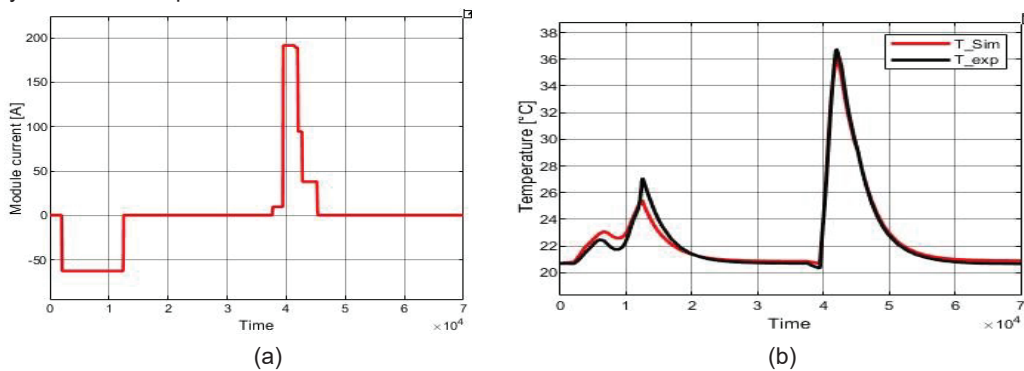


Figure.12. Model validation results: a) Input current, b) cell temperature

In this section a comparison between the three configurations presented in the Fig. 5 has been done in order to assess the benefits of adding the cooling plates regarding the battery module thermal management. According to the Fig.13, the third configuration (module with top and bottom cooling plates) represented by the blue color is the most efficient in term of thermal management, and it's the

best way of extracting and dissipating the calories generated by the battery during charge and discharge. As a consequence, the maximum pick temperature is reduced compared to the configuration represented by the black curve where the module is cooled only by the bottom cooling plate. Also, one can note that the time constant is shortened which proves the efficiency of this configuration.

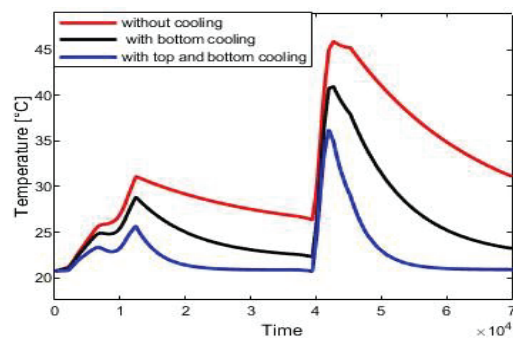


Figure. 13. Thermal management system performance

## 6. Conclusion

In this study, a methodology of battery module modelling is proposed, by taking into account the battery cells, the busbars and also the thermal spacers between the battery cells. A qualitative study is done on a battery module by investigating the benefit of adding the top cooling plate in the overall battery module thermal management. According to simulations and experiments regarding one case study, the configuration with top and bottom cooling plates makes it possible to not only cool the module more quickly by reducing the thermal time constant by 47% but also reduces the battery maximum pick temperature reached with a conventional cooling system by 6°C. Different electrothermal tests have been carried out to validate the battery module model with different scenarios in term of air/coolant temperatures and current profiles in (charge and discharge). It stands out that the model has a good reproducibility, and the error is always below the thermocouple's uncertainty. It stands out also that it gets easier and more efficient to extract calories from the batteries by adding the top cooling plate.

In this paper, only the prismatic cells are concerned, but the methodology can be applied on different battery types and for different battery module topologies.

## Acknowledgments

This work took place in the framework of the OpenLab 'Electronic and Systems for Automotive' combining IMS Laboratory, Lodz Laboratory and Stellantis. This work was carried out under a CIFRE agreement and granted by the ANRT

## Nomenclature

$C_{BB}$	busbar specific heat, J/(kg K)	$h_{conv}$	convective heat transfer coefficient, W/(m <sup>2</sup> K)
$I$	current flowing through the battery and busbar, A		
$I_{CHA}$	charge current, A		
$I_{DIS}$	discharge current, A		
$Q_{dis}$	heat dissipated by the battery, W		
$Q_{irr}$	irreversible heat, W		
$Q_{rev}$	reversible heat, W		
$l_{BBi}$	length of the busbar mesh, m		
$m_{BBi}$	busbar mesh mass, Kg		
$T_b$	battery temperature, K		
$T_{env}$	environment temperature, K		

$Q_{cond}$	heat exchanged with the battery by conduction, W
$Q_{gen}$	heat generated by the battery, W
$R_{th}$	thermal resistance, K/W
$S_{BB}$	cross-sectional area of the busbar, m <sup>2</sup>
$T_A$	ambient temperature, °C
$T_{BBi}$	temperature of the busbar mesh, K
$T_c$	coolant temperature, °C
$T_{neigh}$	neighbour elements of the cells, K

#### Greek symbols

$\rho$  density, Kg/m<sup>3</sup>

#### Subscripts and superscripts

$JR$  jelly roll

$LiBs$  lithium-ion batteries

$OCV$  open circuit voltage

$SoC$  state of charge

$TMS$  thermal management system

## References

- [1] F. Maisel, C. Neef, F. Marscheider-Weidemann, et N. F. Nissen, « A forecast on future raw material demand and recycling potential of lithium-ion batteries in electric vehicles », *Resour. Conserv. Recycl.*, vol. 192, p. 106920, mai 2023, doi: 10.1016/j.resconrec.2023.106920.
- [2] M. Steinhardt, E. I. Gillich, M. Stiegler, et A. Jossen, « Thermal conductivity inside prismatic lithium-ion cells with dependencies on temperature and external compression pressure », *J. Energy Storage*, vol. 32, p. 101680, déc. 2020, doi: 10.1016/j.est.2020.101680.
- [3] Y. Zhou, Z. Wang, Z. Xie, et Y. Wang, « Parametric Investigation on the Performance of a Battery Thermal Management System with Immersion Cooling », *Energies*, vol. 15, n° 7, p. 2554, mars 2022, doi: 10.3390/en15072554.
- [4] I. A. Hunt, Y. Zhao, Y. Patel, et J. Offer, « Surface Cooling Causes Accelerated Degradation Compared to Tab Cooling for Lithium-Ion Pouch Cells », *J. Electrochem. Soc.*, vol. 163, n° 9, p. A1846-A1852, 2016, doi: 10.1149/2.0361609jes.
- [5] X. Feng, C. Xu, X. He, L. Wang, G. Zhang, et M. Ouyang, « Mechanisms for the evolution of cell variations within a LiNi<sub>x</sub>Co<sub>y</sub>Mn<sub>z</sub>O<sub>2</sub>/graphite lithium-ion battery pack caused by temperature non-uniformity », *J. Clean. Prod.*, vol. 205, p. 447-462, déc. 2018, doi: 10.1016/j.jclepro.2018.09.003.
- [6] T. Amalsh et N. Lakshmi Narasimhan, « Liquid cooling vs hybrid cooling for fast charging lithium-ion batteries: A comparative numerical study », *Appl. Therm. Eng.*, vol. 208, p. 118226, mai 2022, doi: 10.1016/j.applthermaleng.2022.118226.
- [7] J. Liu, Y. Fan, et Q. Xie, « Feasibility study of a novel oil-immersed battery cooling system: Experiments and theoretical analysis », *Appl. Therm. Eng.*, vol. 208, p. 118251, mai 2022, doi: 10.1016/j.applthermaleng.2022.118251.
- [8] A. H. Mohammed *et al.*, « Dual-purpose cooling plate for thermal management of prismatic lithium-ion batteries during normal operation and thermal runaway », *Appl. Therm. Eng.*, vol. 160, p. 114106, sept. 2019, doi: 10.1016/j.applthermaleng.2019.114106.
- [9] S. M. Rezvanizani, Z. Liu, Y. Chen, et J. Lee, « Review and recent advances in battery health monitoring and prognostics technologies for electric vehicle (EV) safety and mobility », *J. Power Sources*, vol. 256, p. 110-124, juin 2014, doi: 10.1016/j.jpowsour.2014.01.085.
- [10] R. Gozdur, B. Guzowski, Z. Dimitrova, A. Noury, G. Mitukiewicz, D. Batory. An energy balance evaluation in lithium-ion battery module under high temperature operation. *Energy Conv. and Manag.*, vol. 227, p. 113565, Jan 2021, doi:10.1016/j.enconman.2020.
- [11] S. Madaoui *et al.*, « A detailed Electro-thermal model of an NMC lithium-ion prismatic cell », *VTC2023Spring conference*.